Electronic Supplementary information for

Frequency tuning allows flow direction control in microfluidic network with passive features

Rahil Jain[1] and Barry Lutz[2]

[1]*University of Washington, Department of Electrical Engineering, Seattle, WA 98195*

[2]*University of Washington, Department of Bioengineering, Seattle, WA 98195*

Section 1: Capacitance is halved when a weir is added

Section 2: Adding a port does not affect the frequency response of the underlying microfluidic network

Section 3: AC flow images at f_o and f_p for Device 1 showing comparable flow upstream and downstream. AC flow images at f_o and f_s for Device 2 showing comparable flow upstream and downstream

Section 4: AC flowrate response depicting cancelling flows at parallel resonance

Section 5: Analytical expressions for resonance frequencies

Section 6: Forward pumping at parallel resonance is not possible with any practical device

Section 7: DC Pump pressure vs frequency plots for Device 1 and Device 2

Additional supplementary materials

Supplementary **video** Device 1

Supplementary **video** Device 2

Supplementary **video** Bi-directional pump device

Section 1: Estimation of capacitance due to a weir placed underneath

We created a device (BVD3, Fig. S1a top) identical to the Device 2 (backward flow) from the manuscript, except that there was no weir under the capacitor diode. The device operation was same as described in the main text. Both inlets were left open to air. AC flowrate images were obtained about the center of the upstream channel for a range of frequencies. The images were programmatically analyzed to estimate the upstream AC flowrate frequency response (Fig. S1b) as described previously [Reid, Ref#5 main text].

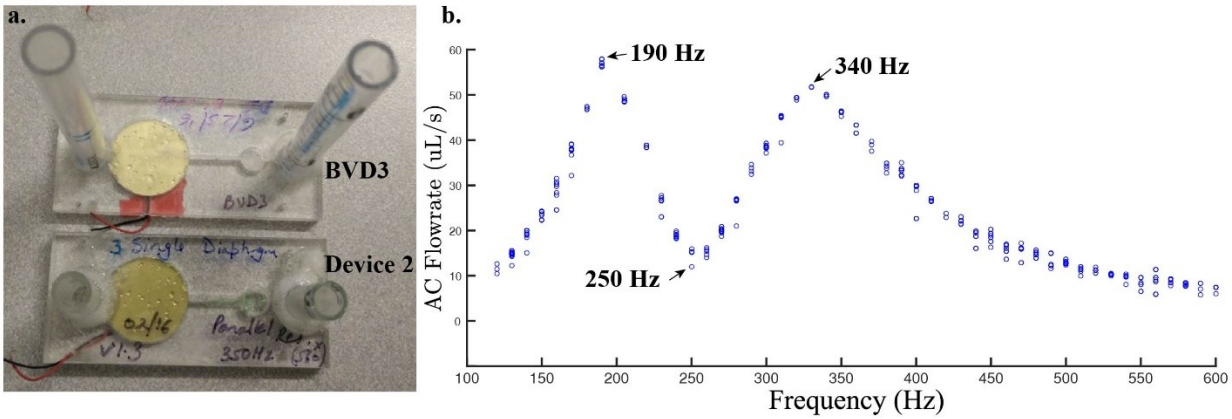

Figure S1: a. Backward pumping device from main text (Device 2, bottom) and an identical device (BVD3, top) without the weir. **b.** Upstream (channel connecting the piezo and the diode capacitor) AC flowrate frequency response shows f_o = 190 Hz, f_p = 250 Hz and f_s = 340 Hz.

Compared to Device 2 (f_o = 200Hz, f_p = 340Hz and f_s = 510 Hz), the parallel and series resonance frequencies for the weir-less device were lower (f_o = 190Hz, f_p = 250Hz and f_s = 340 Hz). We believe that with the weir to impede the bimorph flexing of the diaphragm, the diode capacitance is reduced by half (*i.e.*, $C_{c,\ no\ weir} = 1/2 * C_{c,\ weir}$). The increase in capacitance results in lowering of the resonance frequencies (f_p and f_s). Since f_o does not depend on the capacitor diode (C_c), it remains roughly the same between the two devices. Using the resonance frequency expressions provided in **Section 6**, we can estimate the change in f_p and f_s due to change in diode capacitor C_c only:

Model predicted ratio of parallel resonance f_p:

$$\frac{f_{p,\ Device\ 2}}{f_{p,\ BVD3}} = \frac{\frac{1}{2\pi}\sqrt{\frac{1}{L_d \frac{C_c}{2}}}}{\frac{1}{2\pi}\sqrt{\frac{1}{L_d C_C}}} = \sqrt{2} = \mathbf{1.41}$$

Observed shift in f_p is comparable:

$$\frac{f_{p,\ Device\ 2}}{f_{p,\ BVD3}} = \frac{340\ Hz}{250\ Hz} = 1.36$$

Model predicted ratio of series resonance f_s:

$$\frac{f_{s,\ Device\ 2}}{f_{s,\ BVD3}} = \frac{\frac{1}{2\pi}\sqrt{\frac{-\frac{C_c}{2}L_u R_d^2 + L_u^2 + L_u L_d}{\frac{C_c}{2}L_u L_d^2}}}{\frac{1}{2\pi}\sqrt{\frac{-C_c L_u R_d^2 + L_u^2 + L_u L_d}{C_c L_u L_d^2}}}$$

Generally, $-C_c L_u R_d^2 \ll L_u^2 + L_u L_d$, thus $\frac{f_{s,\ Device\ 2}}{f_{s,\ BVD3}} = \sqrt{2 \times \frac{(L_u^2 + L_u L_d)}{(L_u^2 + L_u L_d)}} = \sqrt{2} = 1.41$

Observed shift in f_s is also comparable: $\frac{f_{s,\ Device\ 2}}{f_{s,\ BVD3}} = \frac{510\ Hz}{340\ Hz} = 1.50$

Thus, the decrease in resonance frequencies (f_p and f_s) can be attributed to the absence of the weir.

Section 2: Adding a port does not affect the frequency response of the underlying microfluidic network

We made two simple devices with only the upstream channel, the piezo buzzer and the channel connecting the piezo buzzer to the inlet on the left. In the bottom device in Fig. S2a (BVD2), a fluid port similar to the devices in the manuscript was added. The left inlet was plugged for the BVD1 device using scotch tape. AC flowrate frequency response (Fig. S2b) was obtained as described in the previous section.

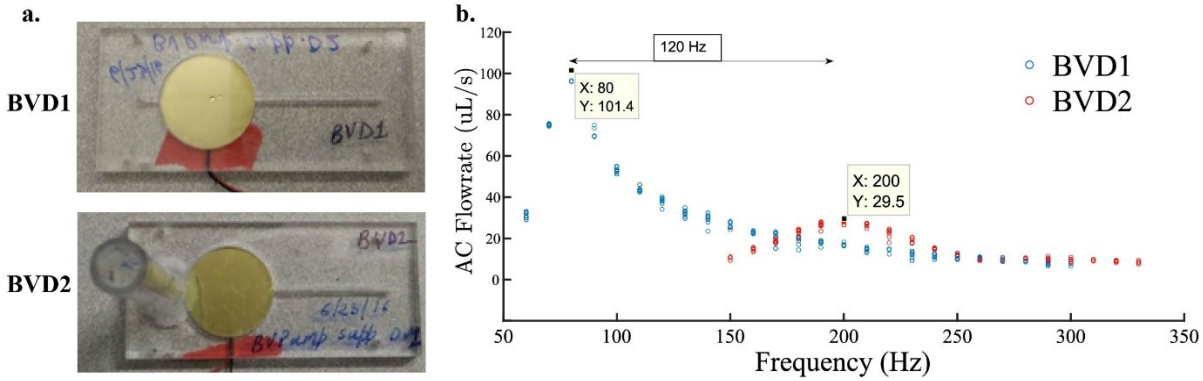

Figure S2: a. BVD1 and BVD2 were identical devices except that BVD2 had a port added to the left. **b.** The AC flowrate frequency response shows f_o series resonance frequencies of 80 Hz and 200 Hz for the BVD1 and BVD2 devices, respectively. Note the reduced magnitude at resonance for the BVD2 device due to the parallel port channel. Upstream channel length: 26.5 mm (model predicted average L = 30.5 µH, R = 0.2 mΩ), inlet channel length: 4.1 mm (L = 4.71 µH, R = 0.1 mΩ) and capacitor radius: 10 mm radius (C_p = 0.132 F). Note: 1 H = kg/mm^4, 1Ω = kPa-s/mm^3 and 1 F = mm^3/kPa.

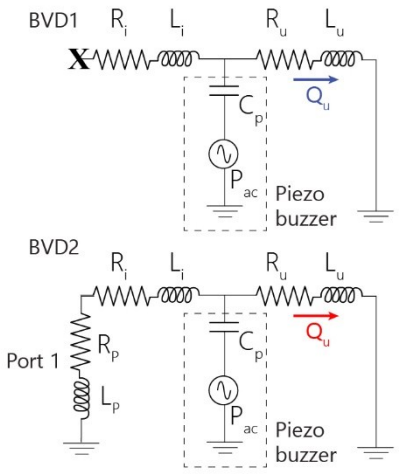

Figure 3: Electrical circuit model for the BVD1 and BVD2 devices. Note, L_s and R_s from the manuscript are made up of the inlet channel impedances (subscript i) and the port impedances (subscript p).

Calculations: Validating model prediction with BVD1

$$f_{o\ BVD1}(model) = {}^{1}\!/_{2\pi\sqrt{L_u C_p}} = {}^{1}\!/_{2\pi\sqrt{30.5\mu \times 0.132}} = 79.3\ Hz$$

$$f_{o\ BVD1}(observed) = 80\ Hz$$

Calculating the unknown port inductance (L_p) by equating model prediction to the observed f_o for BVD2

$$f_{o\ BVD2}(model) = {}^{1}\!/_{2\pi\sqrt{L_{eff} C_p}} \text{ where } L_{eff} = \frac{L_u(L_i + L_p)}{L_u + L_i + L_p}$$

Since the upstream channel is much longer ($L_u \gg L_i + L_p$)

$L_{eff} \sim L_i + L_p$

Now, $f_{o\,BVD2}\,(observed) = 200Hz = {}^{1}\!/_{2\pi\sqrt{L_{eff}C_p}}$

$L_{eff} = 4.79\ \mu H = L_i + L_p = 4.71 + L_{p,}$, therefore $L_p = 0.08\mu H$

The port inductance is small compared to other channels in the device (0.08 µH vs 4.71 µH and 30.5µH). Therefore, the effect of the port on the resonance frequencies of device is small and can be ignored.

Section 3: AC flow images at f_o and f_p for Device 1 showing comparable flow upstream and downstream.

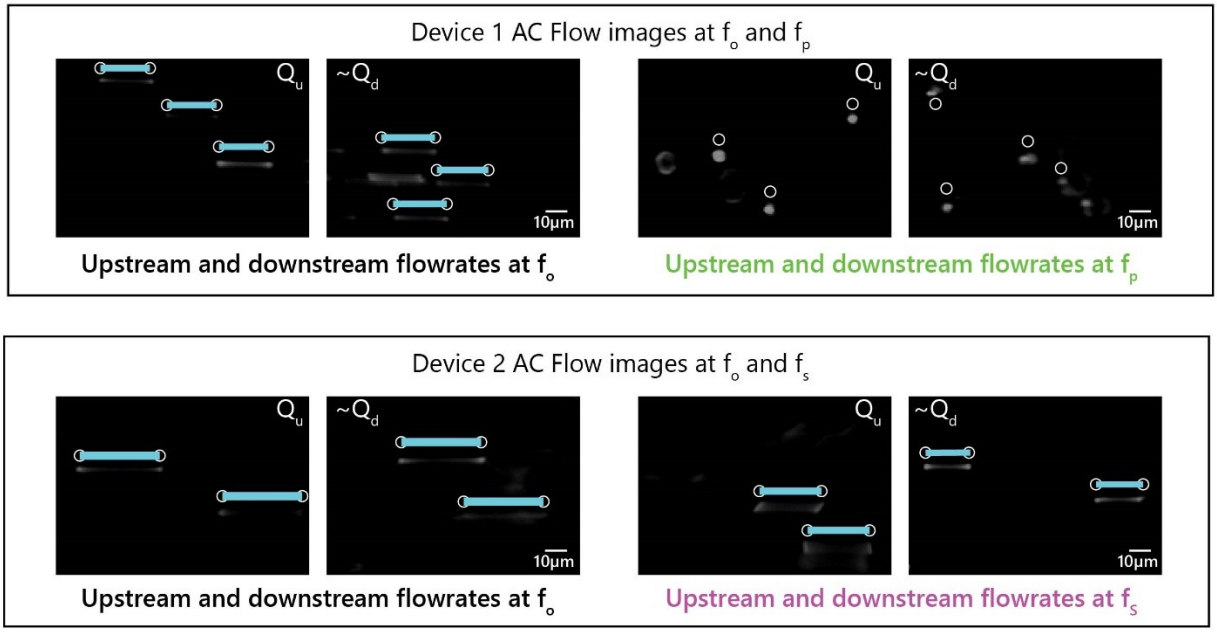

Figure S4: AC Flowrate images show comparable flow in the upstream and downstream channels at non-pumping resonance frequencies. In Device 1, the model predicted significant and comparable Q_u and Q_d at f_o and we observed the same (similar length of bead streaks, top left). Stationary beads indicate no flow at f_p in both the channels ($Q_u \sim Q_d \sim 0$), as expected (top right). Similarly, as per the model, in Device 2 comparable flow was observed at f_o (bottom left) and f_s (bottom right) in both the channels as indicated by similar length bead streaks.

Section 4: AC flowrate amplitude and phase response depicting cancelling flows at parallel resonance

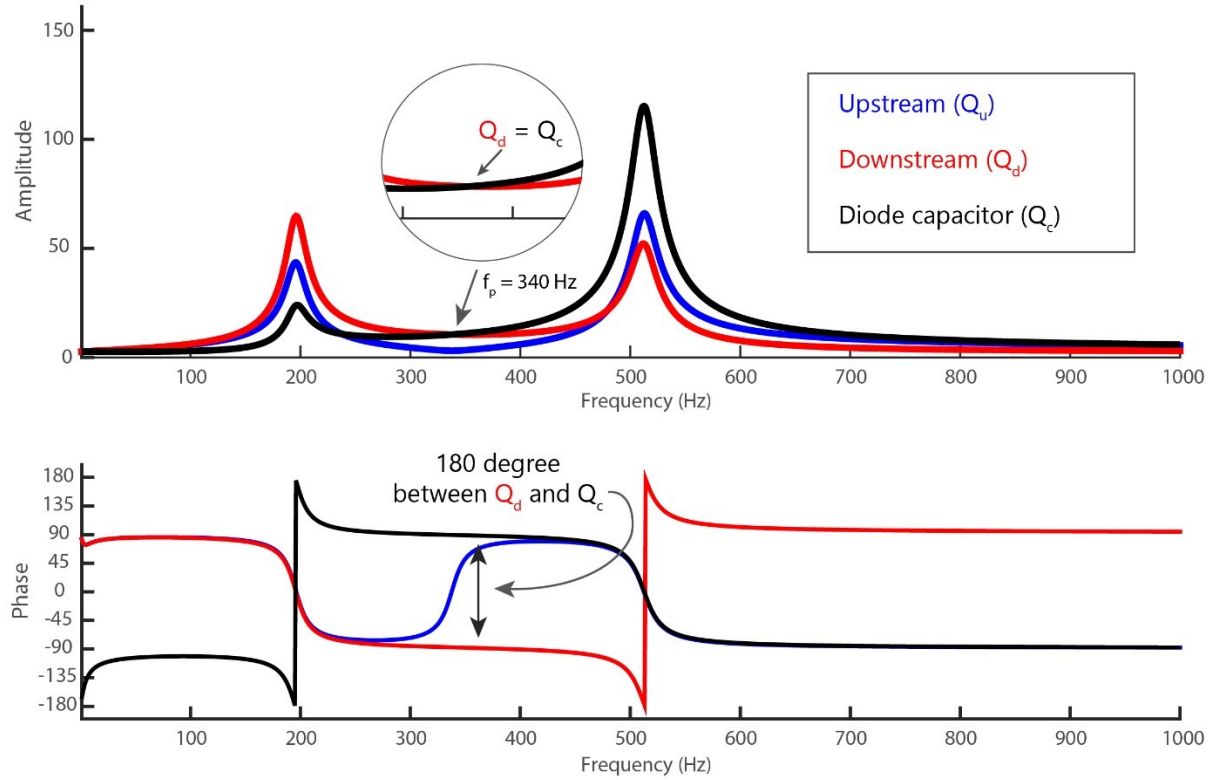

Figure S5: Model predicted AC flowrate amplitude and phase frequency response for Device 2. At f_p = 340 Hz, AC flowrate in the downstream channel and the diode capacitor are equal in magnitude (top, inset) and opposite in phase (180-degree difference in phase, bottom plot).

Section 5 – Analytical expressions for resonance frequencies

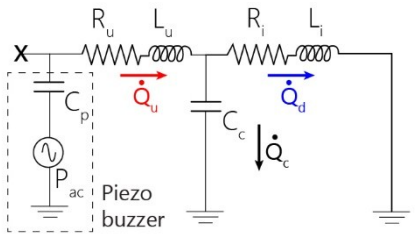

Figure S6: RLC circuit model for a generic microfluidic device with deformable features. Arrows indicate positive flowrate magnitude (not to be confused with flowrate amplitude used in main text)

Referring to the circuit model in Fig. S6, the impedance to the pressure source V_s as a function of excitation frequency can be calculated as series and parallel and combination of the channel and diaphragm impedances as

$$Z_{total} = \frac{1}{j\omega C_p} + (R_u + j\omega L_u) + \frac{\frac{1}{j\omega C_c}(R_d + j\omega L_d)}{\frac{1}{j\omega C_c} + (R_d + j\omega L_d)}$$

Separating Z_{total} into real and imaginary parts, we get

$$Z_{total}|_{Real} = R_u + \frac{R_d}{(C_c L_d \omega^2 - 1)^2 + C_c^2 R_d^2 \omega^2}$$

$$Z_{total}|_{Imag} = \omega L_u - \frac{1}{\omega C_p} + \frac{\omega\left(L_d - C_c R_d^2\right) - C_c L_d^2 \omega^3}{(C_c L_d \omega^2 - 1)^2 + C_c^2 R_d^2 \omega^2}$$

Now, at resonance frequency, $Z_{total}|_{Imag}$ is minimum. Before we differentiate the expression, we note:

- $Z_{total}|_{Imag}$ is independent of R_u. Therefore, we expect that the resonance frequencies will be independent of upstream resistant R_u.
- C_p only appears in the $Z_{total}|_{Imag}$ expression and as an independent term with no interactions suggesting that it may not play an important role in determining resonance frequency points.

At this point, we can easily estimate parallel resonance frequency by looking at the expression for $Z_{total}|_{Real}$. At parallel resonance, the real part of the impedance is maximum. This requires the denominator in the expression for $Z_{total}|_{Real}$ to be minimum. Thus, the squared term in the denominator, $(C_c L_d \omega^2 - 1)^2$, should be equal to zero.

$$C_c L_d \omega_p^2 - 1 = 0$$

$$2\pi f_p = \omega_p = \frac{1}{\sqrt{L_d C_c}}$$

which is same as expression provided in the previous section.

Solving $Z_{total}|_{Imag} = 0$ using the symbolic math toolbox in Matlab yielded three distinct roots. These are the resonance frequency points – f_o, f_p and f_s – shown in the sample AC flowrate frequency response in Fig. 1d. The expressions are too complex and long to include here.

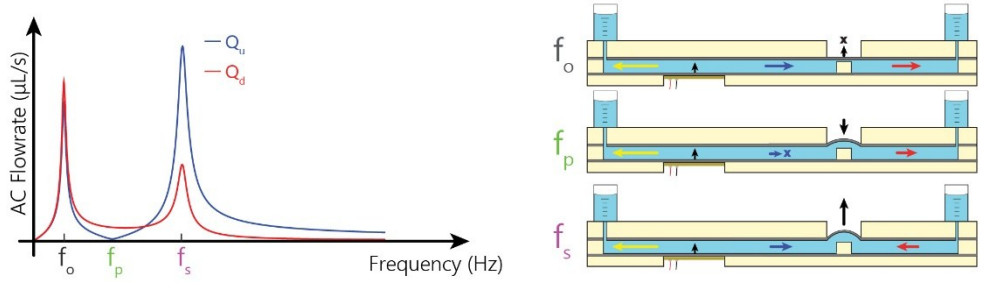

Figure S7: AC flowrate frequency response shows the three distinct resonance points.

We can reduce the expressions for clearer understanding using simple approximation. Since $C_p >> C_c$, the effect of the former can be ignored in the frequency range of operation. Not surprisingly, the expression for $Z_{total}|_{Imag} = 0$ reduces to provide only two frequency points – f_p and f_s – further justifying the rationale that the piezo diaphragm capacitance does not affect the parallel and series resonance of the microfluidic network. We have always observed this experimentally and it was corroborating to note the math works out that way.

Under $C_p >> C_c$ the solution to $Z_{total}|_{Imag} = 0$ becomes

$$\omega = \sqrt{\frac{\pm\left(C_c L_u R_d^2 - L_d^2\right) + L_u^2 + 2L_u L_d - C_c L_u R_d^2}{2L_u L_d^2 C_c}}$$

'+' sign gives the same expression for $\omega = \omega_p$

$$2\pi f_p = \omega_p = \frac{1}{\sqrt{L_d C_c}}$$

'-' sign gives expression for ω_s

$$2\pi f_s = \omega_s = \sqrt{\frac{-C_c L_u R_d^2 + L_u^2 + L_u L_d}{C_c L_u L_d^2}}$$

Note that the expression for series resonance frequency ω_s is independent of R_u. An analysis like Section 1 for series resonance frequency is difficult due to the complex nature of the ω_s expression.

At low frequencies, the diode diaphragm impedance is small ($\frac{1}{\omega C_c} \sim 0$). This is set to zero in the expression for $Z_{total}|_{Imag}$ to get the imaginary part of total impedance at low frequencies -

$$Z_{total}|_{Imag,\ low\ freq} = \omega L_u - \frac{1}{\omega C_s} + \omega L_d$$

Solving for $Z_{total}|_{Imag,\ low\ freq} = 0$ yields a single solution

$$2\pi f_o = \omega_o = \frac{1}{\sqrt{(L_u + L_d)C_p}}$$

which is expected. The resonance frequency f_o depends only on the series sum of channel inductances and the piezo diaphragm capacitance. f_o is primarily decided by C_s as it is orders of magnitude larger than the total inductance of the system. In practice, we observe f_o around 60Hz across all the devices.

Section 6 – Forward pumping at parallel resonance is not possible with any practical device

The mathematical framework showing that at parallel resonance $\dot{Q}_u < \dot{Q}_d$ for devices that can be fabricated using the methods described in the main text.

Figure S8: RLC circuit model for a generic microfluidic device with deformable features

Aim: To show $\left|\frac{\dot{Q}_u}{\dot{Q}_d}\right| < 1$ at f_p for all practical device designs

Note: Effect of diode in the circuit response is ignored for simplicity of calculation. $\dot{Q}$ is flowrate magnitude (not to be confused as amplitude, Q, used in main text)

Using mesh analysis, we write voltage loop equations for the downstream channel and the diode valve to get

$$\dot{Q}_d(R_d + j\omega L_d) - {\dot{Q}_c}/{j\omega C_c} = 0$$

and current conservation gives us $\dot{Q}_u = \dot{Q}_d + \dot{Q}_c$

Eliminating $\dot{Q}_c$ and rearranging gives

$$\frac{\dot{Q}_u}{\dot{Q}_d} = 1 + (R_d + j\omega L_d)j\omega C_c$$

which is complex quantity. The magnitude of the ratio is given as

$$\left|\frac{\dot{Q}_u}{\dot{Q}_d}\right|^2 = (1 - \omega^2 L_d C_c)^2 + (\omega C_c R_d)^2$$

Now, we already know the expression for parallel resonance frequency (derived in previous section):

$$\omega_p = \frac{1}{\sqrt{L_d C_c}}$$

Substituting $\omega = \omega_p$ in the expression for ratio of upstream and downstream flowrate magnitude squared gives

$$\left|\frac{\dot{Q}_u}{\dot{Q}_d}\right|^2_{\omega_p} = (1 - \frac{1}{L_d C_c} L_d C_c)^2 + (\frac{1}{\sqrt{L_d C_c}} C_c R_d)^2$$

$$\left|\frac{\dot{Q}_u}{\dot{Q}_d}\right|_{\omega_p} = R_d\sqrt{\frac{C_c}{L_d}}$$

Since the goal is to understand the relationships between the device dimensions and the frequency response, simplified expressions for R_d and L_d [Morris and Forster, Ref#7 main text] can be used to assess the expression further. Now,

$$R_d = \frac{12\mu l}{w^2 d^2}$$

$$L_d = \frac{\rho l}{wd}$$

Also, $$2\pi f_p = \omega_p = \frac{1}{\sqrt{L_d C_c}}$$

where l, w, and d are length, width and depth of a channel. Fluid dynamic viscosity and density are μ and ρ. Substituting these expressions in the expression for upstream and downstream flowrate ratio at parallel resonance, we get

$$\left|\frac{\dot{Q}_u}{\dot{Q}_d}\right|_{\omega_p} = \frac{2.1}{f_p A} < 1$$

Where A= w*d is the cross-sectional area of the channel.

It is important to note that the flowrate ratio is inversely proportional to the cross sectional area of the channel and the parallel resonance frequency. In our work, we aim for device operation in audio frequency range (>100Hz) because the broader goal of our research is to control microfluidic devices using audio tones generated on a cellphone (>100 Hz).

For $f_{p,min}$ = 100Hz, the expression reduces to

$$\frac{2.1}{100.A} < 1$$

Or $$A > 0.021 mm^2$$

For a square channel, it is $$w_{min} = d_{min} > 0.14\ mm$$

This implies if channels wider and deeper than 0.14 mm are used, the upstream flow will always be less than downstream flow at parallel resonance frequency. The minimum channel width that could be reliably fabricated using our CO_2 laser cutter (Universal laser systems VLS 3.60) is about 0.8 mm. Hence, the upstream flowrate will always be smaller than the downstream flowrate at parallel resonance frequency for all practical devices using the described fabrication methods. **Example**: For the range of device geometries and diaphragm material and operation in the 100-2000 Hz frequency range, the model-predicted magnitude order for $R_d \sim 10^{-3}$ kPa-s/mm^3, $C_c \sim 10^{-3}$-10^{-2} mm^3/kPa and $L_d \sim 10^{-5}$ Kg/mm^4. For these typical values, $$\left|\frac{\dot{Q}_u}{\dot{Q}_d}\right|_{\omega_p} \sim 10^{-3}\sqrt{\frac{10^{-2}}{10^{-5}}} = 10^{-1.5} \ll 1$$

Section 7 – DC Pump pressure vs frequency plots for Device 1 and Device 2

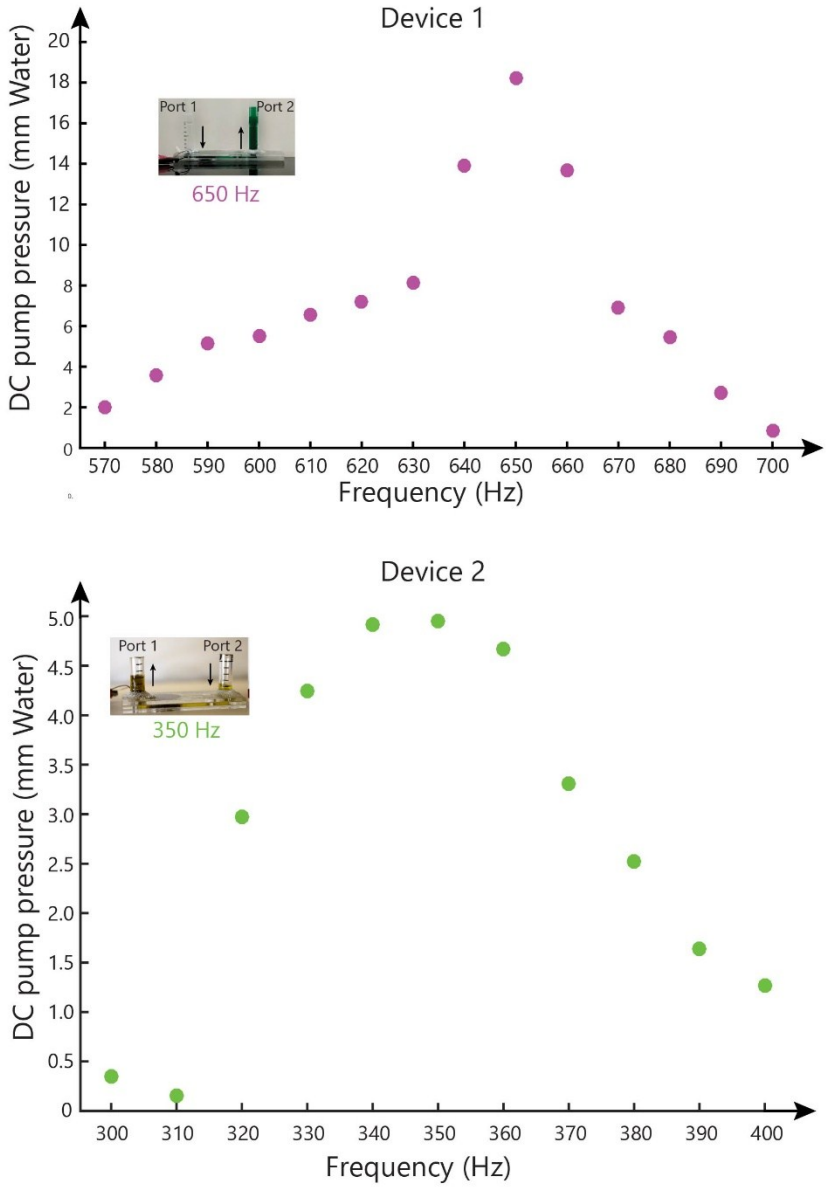

Figure 9: DC Pump pressure frequency responses for Device 1 and Device 2 show the same peak frequencies as the DC flowrate response included in the main text. The peak DC flowrate and DC pump pressure may be inversely related. Device 2 had lower DC pump pressure (18.44 mm H_20 vs 4.9 mm H_20), but higher DC flowrate compared to Device 1 (2.5 µL/s vs 4.2 µL/s). Understanding the relationship between the DC pump pressure and DC flowrate may be imperative to designing more efficient direction control frequency-tuned pumps.